Four-dimensional topological Anderson insulator with an emergent second Chern number

Rui Chen,* Xiao-Xia Yi, and Bin Zhou†
Department of Physics, Hubei University, Wuhan 430062, China

(Received 30 June 2023; accepted 21 August 2023; published 29 August 2023)

Four-dimensional (4D) topological insulators, which are impossible in real materials, have attracted much attention by virtue of the recent progress achieved in quantum simulations of higher-dimensional systems. In this paper, we employ the supercell approximation to investigate the disorder effects on a system that supports the 4D topological insulator phases characterized by quantized second Chern numbers and the normal insulator phase. We demonstrate that the 4D topological insulator phases are robust against weak disorders. Moreover, we reveal that disorder can transform a normal insulator to a 4D topological insulator with an emergent second Chern number, referred to as a 4D topological Anderson insulator. An effective-medium theory based on the Born approximation further confirms the numerical conclusions.

DOI: 10.1103/PhysRevB.108.085306

I. INTRODUCTION

Since the discovery of topological insulators [1–4], tremendous effort has been devoted to generalizing the exotic phase of matter to higher dimensions [5–23]. Recently, significant advances have been achieved in the field of quantum simulation of higher-dimensional systems ($d \geqslant 4$), such as four-dimensional (4D) topological insulators in optical lattices [24], photonic systems [25], acoustic lattices [26], and electric circuits [27,28], which led to a surge of interest in higher-dimensional topological phases [29–34]. 4D topological phases are characterized by the second Chern number [35–38], a topological invariant that appears in the quantization of the transverse conductivity for the nonlinear response. Moreover, research into higher-dimensional systems has provided valuable insight into the topological phenomena observed in two-dimensional (2D) quasicrystals [39,40] and hyperbolic lattices [41,42].

On the other hand, disorder plays a significant role in determining the transport properties of low-dimensional electronic systems. The topological Anderson insulator (TAI) is a type of disorder-induced phase with remarkable topologically nontrivial properties, which was proposed by Li *et al.* [43]. Since then, the disorder-induced topological phases have been investigated in various low-dimensional systems [44–59]. So far, the TAI phase had been observed experimentally in one-dimensional (1D) disordered atomic wires [60], photonic platforms [61–63], and a quantum simulator on a superconducting-circuit device [64]. Recently, the TAI phase was proposed to be realized in an electric circuit [65]. Then a question naturally arises whether such an exotic phase can occur in higher dimensions and differ from its low-dimensional counterpart. However, the demanding computation requirement has hindered the further exploration on disorder effects in higher dimensions.

In this paper, we adopt a supercell approximation to investigate the disorder effects on a 4D system. Depending on the value of the Dirac mass, the system supports both the normal insulator phase with a zero topological index and the 4D topological insulator phase characterized by a nonzero second Chern number. We first show that the 4D topological insulator phase is robust against weak disorder. Then we find that disorder can induce a phase transition from a normal insulator phase to a topological insulator phase with an emergent second Chern number $C_2 = 1$, indicating the occurrence of the 4D TAI phase. Moreover, we find disorder can also transform a topological insulator phase with $C_2 = 1$ to another topological phase with a higher second Chern number $C_2 = -3$. The disordered phase diagram is explained based on using the Born approximation method. Finally, the disorder-induced topological phase transition is further confirmed by calculating the disorder-averaged local density of states.

II. MODEL AND TOPOLOGICAL INDEX

A. Model

We start with the Dirac model describing the 4D topological insulator [35,36]:

$$H = \sum_i d_i(\mathbf{k})\Gamma^i, \tag{1}$$

with $d(\mathbf{k}) = [(m + c\sum_i \cos k_i),\ \sin k_x,\ \sin k_y,\ \sin k_z,\ \sin k_w]$ as a five-dimensional vector. The parameter m determines the value of the Dirac mass. The Dirac matrices $\Gamma = (s_x s_0, s_y s_0, s_z s_x, s_z s_y, s_z s_z)$ satisfying the anticommutation relations $\{\Gamma^\mu, \Gamma^\nu\} = 2\delta_{\mu\nu}$, where $s_{x,y,z}$ are Pauli matrices and s_0 is an identity matrix. The bulk spectrum of the system has the form $E_\pm = \pm\sqrt{\sum_{i=1}^{5} d_i(\mathbf{k})}$, with both eigenvalues being doubly degenerate. The system is always gapped at half-filling, except for some special points at $m/c = \pm 2, \pm 4$, and 0.

*chenr@hubu.edu.cn
†binzhou@hubu.edu.cn

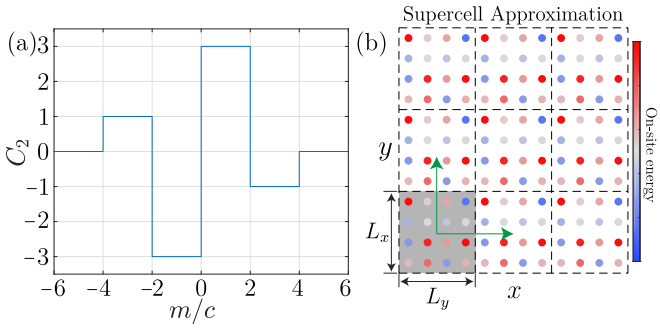

FIG. 1. (a) The second Chern number C_2 as a function of the parameter m/c. (b) Schematic illustration of the supercell approximation in two dimensions. Here, the color indicates the strength of the on-site energy. The region colored by gray corresponds to a super unit cell.

B. Second Chern number

In 4D, the response of the current to an electric field **E** and a magnetic field **B** is related to two kinds of topological invariants. The linear and nonlinear responses are related to the total Chern number and the total second Chern number, respectively. The second Chern number is obtained by numerically calculating the following formula [35]:

$$C_2(\varepsilon_F) = \frac{1}{4\pi^2}\int_{\mathrm{FBZ}} d\mathbf{k}\,\mathrm{Tr}[F_{xy}F_{zw} + F_{wx}F_{zy} + F_{zx}F_{yw}], \quad (2)$$

where the non-Abelian Berry curvature $[F_{lm}(\mathbf{k})]^{\alpha\beta} = \partial_{k_l}A^{\alpha\beta}_{k_m}(\mathbf{k}) - \partial_{k_m}A^{\alpha\beta}_{k_l}(\mathbf{k}) + i[A_{k_l}, A_{k_m}]^{\alpha\beta}$ is written in terms of the Berry connection of the occupied bands $A^{\alpha\beta}_{k_m}(\mathbf{k}) = i\langle\psi^\alpha(\mathbf{k})|\nabla_{k_m}|\psi^\beta(\mathbf{k})\rangle = \frac{i\langle\psi^\alpha|\partial H/\partial k_m|\psi^\beta\rangle}{E_\alpha - E_\beta}$, and the trace is taken over the occupied bands [36,38,42].

Figure 1(a) shows the numerically calculated second Chern number C_2 as a function of the Dirac mass m. The system is topologically trivial with $C_2 = 0$ when $|m/c| > 4$, supports the topological phase characterized by quantized second Chern numbers $C_2 = \pm 1$ when $2 < |m/c| < 4$, and has topological phases with higher second Chern numbers $C_2 = \pm 3$ when $|m/c| < 2$. In Appendix A, we calculate the spectrum of the 4D system and provide more details on the bulk-boundary correspondence of the topological phases characterized by quantized Chern numbers.

C. Supercell approximation

In general, disorder effects in topological insulators can be studied in either momentum space [66] or real space [67–69]. A drawback of studying disorder effects in momentum space is that the stability of a topological state can only be calculated perturbatively [66]. Computations in real space apply to the disorder of arbitrary strengths, but this often requires significant computational resources. Disorder effects in lower-dimensional topological insulators have been widely studied by adopting real-space techniques [70–83]. However, the demanding computation requirement and a lack of computing method for the real-space second Chern number has hindered its further exploration in higher dimensions.

Here, we adopt the supercell approximation to investigate the disorder effects in the 4D system. This can be understood from Fig. 1(b), where a 2D supercell system is illustrated. The real-space configurations are approximately investigated by considering a supercell within the first Brillouin zone (FBZ). The quantities calculated in real space can be accurately approximated with the increasing supercell size. Moreover, the supercell approximation has been adopted in various disordered systems [84–88].

In Appendix B, we investigate the disorder effects on a 2D Dirac model that supports the 2D topological insulator phase. We compare the results obtained by calculating the Bott index in the real space and the results obtained by calculating the Chern number in a supercell system. In the presence of disorder, the results obtained via the supercell approximation can reproduce that by calculating the Bott index in the real space. Moreover, the supercell approximation requires much less memory than the calculations in the real space. These features provide the possibility to study the disorder effects in higher-dimensional systems.

III. DISORDER EFFECT

Now we investigate disorder effects on the 4D system in Eq. (1) by adopting the supercell approximation. In the numerical calculations, we discretize the effective Hamiltonian on a 4D hypercubic lattice and set the lattice constants as $a = 1$. The volume of the 4D supercell is $V = L_xL_yL_zL_w$, where $L_{x,y,z,w} = n_{x,y,z,w}a$ are the side lengths of the hypercube, and $n_{x,y,z,w}$ correspond to the numbers of lattice sites. We adopt the Anderson-type disorder by considering random on-site energies fluctuating in the energy interval $[-W, W]$, where W is the disorder strength. The k points used in the integrals in Eq. (2) are 20^4 in the 4D Brillouin zone.

A. Numerical results obtained by supercell approximation

We first study the disorder effects on two topologically nontrivial cases. In the clean limit, the 4D topological insulator is characterized by quantized second Chern numbers $C_2 = 1$ and -3 for $m/c = -3.5$ and -1.5, respectively [Fig. 1(a)]. With increasing disorder strength, C_2 keeps the quantized value until the disorder strength exceeds about $W/c = 3$ [Fig. 2(a)]. Therefore, like the previous studies on disordered topological systems [43,44], the topological nature of the 4D topological insulator is robust against disorder. Further increasing the disorder strength, the quantized C_2 is suppressed by disorder, then gradually decreases and finally collapses to zero.

For a topologically trivial phase with $m/c = -4.2$, in the clean limit, the system is characterized by $C_2 = 0$ [Fig. 2(b)]. With increasing disorder strength, the disorder-averaged second Chern number C_2 increases and then forms a quantized plateau with $C_2 = 1$. The quantized plateau is observed for a certain range of disorder strength, and it decreases and finally disappears with increasing the disorder strength. The zero conductance fluctuation of the quantized plateau indicates that it may be a topological phase. Moreover, we find disorder can also induce a phase transition. When $m = -2.2$, the system is characterized by $C_2 = 1$ in the clean limit. With increasing

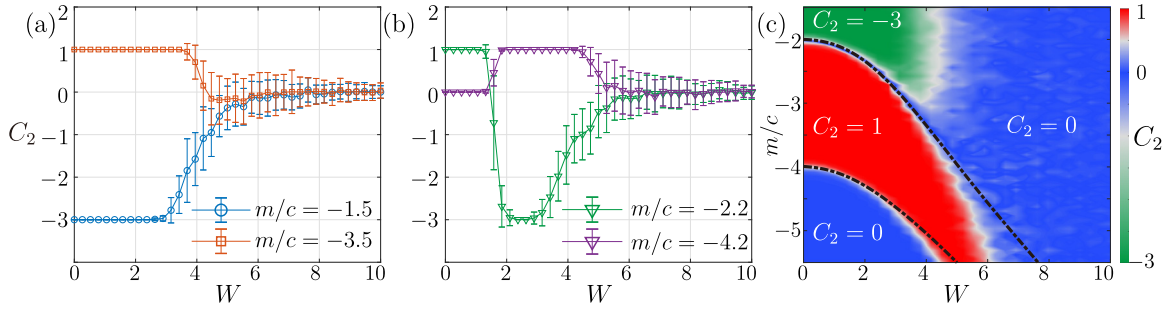

FIG. 2. (a) and (b) Disorder-averaged second Chern number as a function of disorder strength W for different Dirac mass m. (c) Disorder-averaged second Chern number as a function of m and W. Here, the black dashed lines are obtained by Born approximation in Eq. (3). In the numerical calculations, the system size is taken as $L_{x,y,z,w} = 3$. Each point is obtained after averaged on 200 independent disorder configurations. In (a) and (b), the Fermi energy E_F is taken as $E_F = 0$.

disorder strength, C_2 drops and reaches another quantized plateau with $C_2 = -3$.

In Fig. 2(c), we plot the diagrams of the system as a function of m and U. The disorder-induced topological phase transitions can be observed more clearly. In Appendix C, we investigate the finite-sized effect of the 4D system and show that a system size of $L_{x,y,z,w} = 3$ is enough to capture essential features of the disorder-induced phase transitions in the 4D system.

B. Born approximation

To corroborate the physical interpretation of numerical simulation, we analyze the present model within an effective medium theory based on the Born approximation in which high-order scattering processes are neglected [45]. In the self-consistent Born approximation, the self-energy Σ for a finite disorder strength is given by the following integral equation:

$$\Sigma = \frac{W^2}{3}\left(\frac{a}{2\pi}\right)^d \int_{\mathrm{FBZ}} d\mathbf{k} \frac{1}{E_F - H(\mathbf{k}) - \Sigma}, \tag{3}$$

where $H(\mathbf{k})$ is the model Hamiltonian of the system and d is the dimension. The coefficient $\frac{1}{3}$ originates from the variance $\langle W^2 \rangle = W^2/3$ of a random variable uniformly distributed in the range $[-W, W]$. This integration is over the FBZ. We will use the lowest-order Born approximation, which means setting $\Sigma = 0$ on the right-hand side of Eq. (3).

Through numerical calculations, we find the self-energy has the following form:

$$\Sigma = \Sigma_0 I_4 + \Sigma_1 \Gamma_1, \tag{4}$$

where I_4 is an identity matrix. This means the Fermi energy E_F and Dirac mass m are renormalized by disorder. Then the effective Fermi energy and effective Dirac mass have the form $\tilde{E}_F = E_F - \Sigma_0$ and $\tilde{m} = m + \Sigma_1$. By calculating the topological properties of the renormalized Hamiltonian, we can obtain the phase boundaries in Fig. 2(c). The two black lines correspond to points where the energy gap is zero, which depict the phase transition lines between two different topological phases, and are determined by calculating the corresponding second Chern number of the occupied bands. Specifically, the lower black line corresponds to a band inversion at the Γ point (see Appendix A), which separates the normal insulator phase with $C_2 = 0$ and the topological phase with $C_2 = 1$. The upper black line corresponds to band inversions at M points, which separates the two topological phases with $C_2 = 1$ and -3. The results based on the Born approximation fit well with the numerical calculations for weak disorders, which confirms that disorder has a renormalization effect on the system parameters, leading to the various topological phase transitions in the 4D system. Therefore, we identify this disorder-induced topological phase as a 4D TAI phase.

C. Local density of states

As shown in Fig. 3(a), the 4D system can be regarded as a quasi-1D system with each site representing a three-dimensional (3D) cube. As illustrated in Appendix A, the 4D TAI phase is expected to demonstrate boundary states along the w direction.

Figure 3(b) shows the disorder-averaged local density of states $D(w)$ as a function of the coordinate w for the 4D TAI phase, where $D(w) = \sum_{x,y,z} D(x, y, z, w)$ is the total density of states of each cube, $D(x, y, z, w) = -\frac{1}{\pi}\mathrm{Im}G^r(x, y, z, w)$ is the local density of states on each site, and $G^r(x, y, z, w)$ is the retarded Green's function obtained by the recursive Green's function method. As expected, the disordered system exhibits localized states near the two boundaries along the w direction, which further confirms that the system corresponds to a topologically nontrivial phase. Moreover, $D(w)$ exhibits a nonvanishing local density of states at the bulk. This phenomenon is also observed in the 2D TAI phase, and we confirmed that they originate from the disorder-induced bulk localized states.

It should be noticed that the local density of states at the boundary should always be larger than that within the bulk region. To eliminate the contribution of the bulk, we plot $D(w) - D(25)$ as a function of w in Fig. 3(c), where $D(25)$ corresponds to the bulk contribution. The density of states of the boundary states increases as the system size grows. This procedure allows us to distinguish between the contributions from the bulk and the boundary states.

IV. CONCLUSIONS

In this paper, we adopt the supercell approximation to investigate the disorder effects in a 4D system. We show that the 4D topological insulator phase, which is characterized

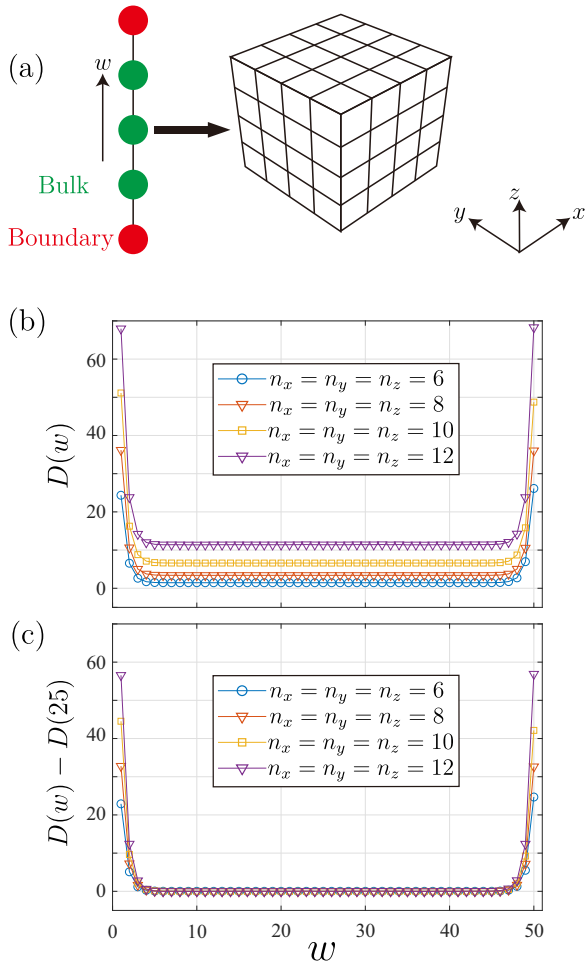

FIG. 3. (a) The four-dimensional (4D) system can be regarded as a quasi-one-dimensional (1D) system with each site representing a three-dimensional (3D) cube. Here, the red and green sites correspond to the boundary and the bulk of the quasi-1D system. (b) The disorder-averaged local density of state $D(w)$ of the 4D topological Anderson insulator (TAI) phase within the quasi-1D geometry shown in (a). (c) is the same as (b), except that the vertical axis corresponds to $D(w) - D(25)$. Here, the parameters are $m/c = -4.2$ and $W = 3$. The length of the quasi-1D system is $n_w = 50$. We take open boundary conditions along the w direction and periodic boundary conditions along the x, y, and z directions.

by a quantized second Chern number, is robust against weak disorder. Moreover, the disorder can also trigger a topological phase transition from a normal insulator to a 4D topological insulator, leading to the 4D TAI phase with an emergent second Chern number. Furthermore, the 4D TAI phase is explained by the self-consistent Born approximation. We also calculate the disorder-averaged density of states, which further confirms that the 4D TAI phase arises from the boundary states induced by disorder.

In addition, we expect the 4D TAI phase can be experimentally realized in an electric circuit, considering the 4D topological insulator [27,28] and the 2D TAI [65] have been realized and proposed in electric circuits, respectively. The hopping terms in the tight-binding Hamiltonian of the system in Eq. (1) are either purely real or purely imaginary, which can be experimentally realized in a four-subnode LC circuit [89]. The disorder effects can be introduced by considering the random-inductance-induced on-site potential [65]. The disorder-induced boundary state as well as the TAI phase can be experimentally detected by directly measuring the impedance in circuits [65]. Therefore, all of these features offer the possibility of realizing our proposal in the future.

ACKNOWLEDGMENTS

R.C. acknowledges the support of NSFC (under Grant No. 12304195) and the Chutian Scholars Program in Hubei Province. B.Z. was supported by the NSFC (under Grant No. 12074107), the program of outstanding young and middle-aged scientific and technological innovation team of colleges and universities in Hubei Province (under Grant No. T2020001), and the innovation group project of the Natural Science Foundation of Hubei Province of China (under Grant No. 2022CFA012).

APPENDIX A: BULK-BOUNDARY CORRESPONDENCE

The bulk-boundary correspondence is one of the most salient features of topologically ordered phases of matter [90,91]. In general, a nonzero topological index indicates the emergence of the boundary states. Next, we investigate the energy spectrum of the 4D system with open boundary conditions along the w direction and periodic boundary conditions along the x, y, and z directions. The system can be treated as a quasi-1D system, and k_x, k_y, and k_z are regarded as tuning parameters. At $k_y = k_z = 0$, gapless boundary modes appear inside the bulk energy gap at $k_x = 0$ ($k_x = \pi$) for the topological phase with $m = -3.5$ ($m = -1.5$) characterized by nonzero second Chern number $C_2 = 1$ ($C_2 = -3$) [Figs. 4(b) and 4(c)]. For the trivial case with $m = -4.5$ and $C_2 = 0$, there is no boundary state [Fig. 4(a)].

In 2D topological phases, the value of the Chern number determines the number of edge states. Similar phenomena are also observed in the 4D system. Figures 4(d) and 4(e) show the value of the energy gap of the quasi-1D system in the (k_x, k_y, k_z) space. For $m = -3.5$ with $C_2 = 1$, the gapless boundary states cross at the Γ point of the Brillouin zone center [Fig. 4(d)]. For $m = -1.5$ with $C_2 = -3$, the gapless boundary states cross at the three M points of the Brillouin zone boundary [Fig. 4(e)]. The above results are in accordance with previous studies [35].

APPENDIX B: DISORDER EFFECTS IN 2D TOPOLOGICAL INSULATOR

1. Model

Here, we study the disorder effects in a 2D topological insulator [35]:

$$H = [m + c(\cos k_x + \cos k_y)]\sigma_z + \sin k_x \sigma_x + \sin k_y \sigma_y, \quad \text{(B1)}$$

where $\sigma_i (i = x, y, z)$ are Pauli matrices describing the spin. In the following calculations, we fix the parameter as $c = 1$. The topological properties of the 2D system are characterized by

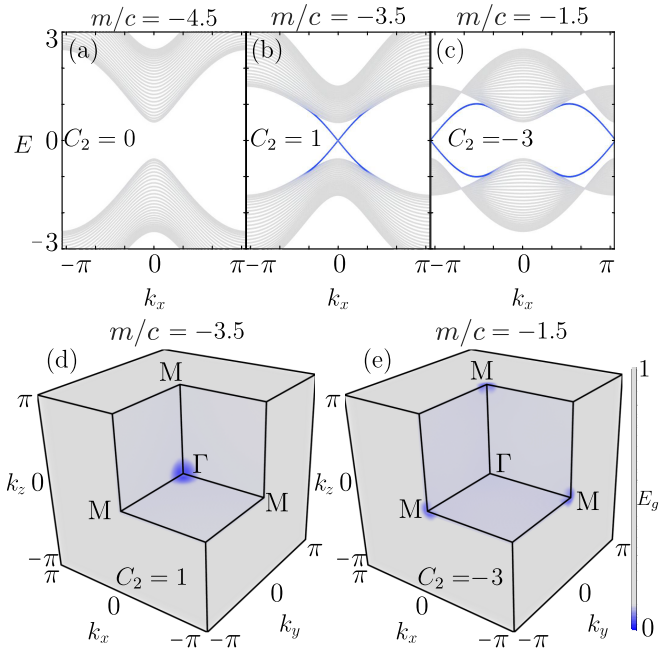

FIG. 4. Energy spectra as a function of k_x at $k_y = k_z = 0$ with Dirac mass (a) $m = -4.5$, (b) $m = -3.5$, and (c) $m = -1.5$. Blue and gray correspond to the boundary and bulk states, respectively. (d)–(e) Energy gap in the (k_x, k_y, k_z) space. In (a)–(e), we take open boundary conditions along the w direction and periodic boundary conditions along the x, y, and z directions.

the Chern number, which is given by [36]

$$C_1 = \frac{1}{2\pi i}\int_{\mathrm{FBZ}} d\mathbf{k}\,\mathrm{Tr}\,F_{xy}. \tag{B2}$$

Figure 5(a) shows the Chern number C_1 as a function of the Dirac mass m. The system is topologically trivial with $C_1 = 0$ when $|m/c| > 2$ and topologically nontrivial with $C_1 = \pm 1$ when $|m/c| < 2$.

In the numerical calculations, we discretize the effective Hamiltonian on a 2D square lattice and set the lattice constants as $a = 1$. The area of the supercell is $V = L^2$, and $L = na$ is the side length. In the numerical calculations, the k points used in the integrals in Eq. (B2) are 20^2 in the 2D Brillouin zone. We adopt the Anderson-type disorder by considering random on-site energies fluctuating in the energy interval $[-W, W]$, where W is the disorder strength.

2. Bott index

The topological property of the disordered 2D system can be characterized by the Bott index [73]. The Bott index is equivalent to the real-space Chern number, which determines the Hall conductivity of the system [92]. Considering two diagonal matrices $X_{i,i} = x_i$ and $Y_{i,i} = y_i$, where (x_i, y_i) are coordinates of the ith lattice, one can obtain the two unitary matrices $U_X = \exp(i2\pi X/L)$ and $U_Y = \exp(i2\pi Y/L)$. Using the eigenstates of the bands below the resonant gap, one obtains the projector P and the projected unitary matrices with $\tilde{U}_{X,Y} = PU_{X,Y}P$. For every random disorder configuration, the Bott index $B = (1/2\pi)\mathrm{Im}[\mathrm{Tr}(\ln\tilde{U}_Y\tilde{U}_X\tilde{U}_Y^\dagger\tilde{U}_X^\dagger)]$ is an integer,

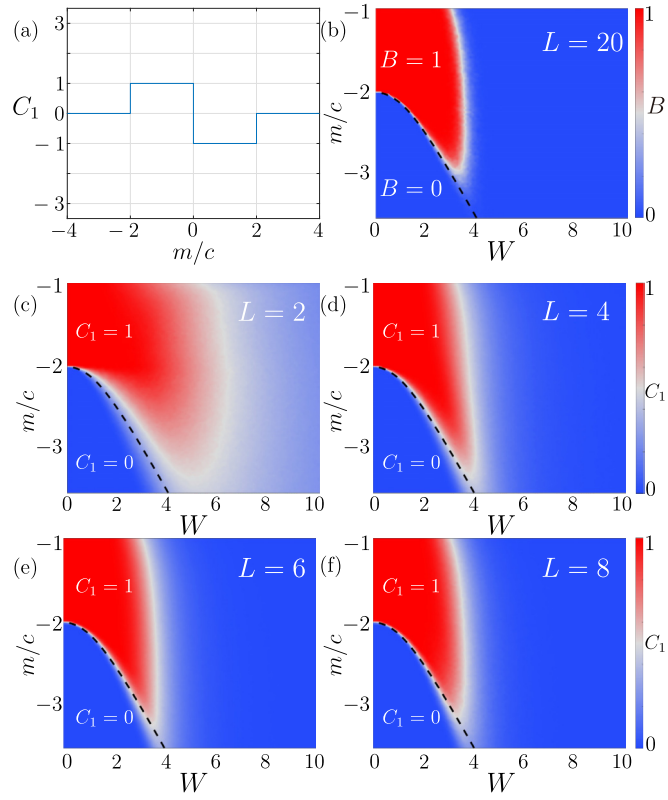

FIG. 5. (a) The Chern number C_1 as a function of m/c for the two-dimensional (2D) topological insulator with $W = 0$. (b) Disorder-averaged Bott index B as a function of the disorder strength W and m/c with side length $L = 20$. Disorder-averaged Chern number C_1 as a function of W and m/c with different side lengths (c) $L = 2$, (d) $L = 4$, (e) $L = 6$, and (f) $L = 8$. In (c)–(f), the k points used in the calculations are 20^2 in the 2D Brillouin zone. In (b)–(f), the black dashed lines are obtained by the Born approximation in Eq. (3).

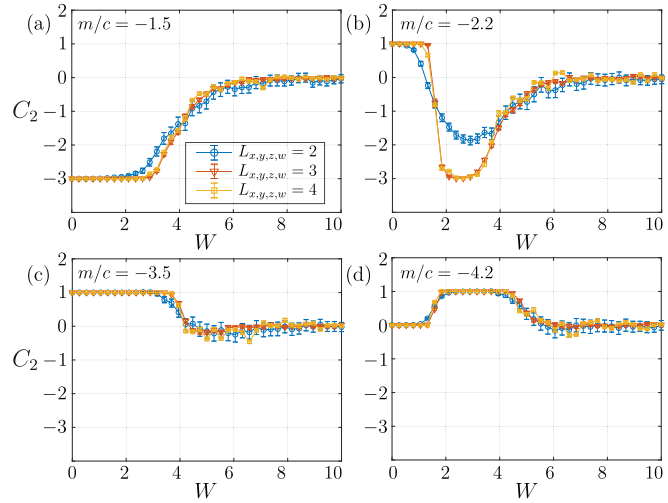

FIG. 6. Disorder-averaged second Chern number C_2 as a function of disorder strength W for different supercell sizes with (a) $m/c = -1.5$, (b) $m/c = -2.2$, (c) $m/c = -3.5$, and (d) $m/c = -4.2$. Here, each point is obtained after averaged on 200 (10) disorder configurations for $L_{x,y,z,w} = 2, 3$ ($L_{x,y,z,w} = 4$).

and the averaged Bott index is computed by averaging various disorder configurations until it converges.

We find that the real-space Bott index obtained in the clean limit is in accordance with the k-space Chern number obtained by using Eq. (B2). Moreover, Fig. 5(b) shows the disorder-averaged Bott index B as a function of m and W. The numerical results are further confirmed by the Born approximation.

3. Supercell approximation

Figures 5(c)–5(f) show the disorder-averaged Chern number C_1 as a function of W and m with different L. The result obtained when $L = 2$ provides a qualitative description of the disorder effects on the 2D system. Upon increasing the system size to $L = 4$, the results are in quantitative agreement with that obtained by calculating the Bott index. As the system size continues to increase, the conclusions drawn from the supercell approximation approach increasingly align with those obtained from the Bott index method. Consequently, we believe the supercell approximation method can characterize disorder effects on topological insulators.

APPENDIX C: FINITE-SIZED EFFECT

Figure 6 shows the disorder-averaged second Chern number C_2 as a function of disorder strength W for different supercell sizes. The finite-sized effect is significant for $L_{x,y,z,w} = 2$ but much weaker for $L_{x,y,z,w} = 3$ and $L_{x,y,z,w} = 4$. The results show that a system size of $L_{x,y,z,w} = 3$ is enough to capture the essential features of the disorder-induced phase transitions in the 4D system.

[1] M. Z. Hasan and C. L. Kane, Colloquium: Topological insulators, Rev. Mod. Phys. **82**, 3045 (2010).

[2] X.-L. Qi and S.-C. Zhang, Topological insulators and superconductors, Rev. Mod. Phys. **83**, 1057 (2011).

[3] S.-Q. Shen, *Topological Insulators* (Springer, Singapore, 2017).

[4] B. A. Bernevig and T. L. Hughes, *Topological Insulators and Topological Superconductors* (Princeton University Press, Princeton, 2013).

[5] B. I. Halperin, Possible states for a three-dimensional electron gas in a strong magnetic field, Jpn. J. Appl. Phys. **26**, 1913 (1987).

[6] G. Montambaux and M. Kohmoto, Quantized Hall effect in three dimensions, Phys. Rev. B **41**, 11417 (1990).

[7] M. Kohmoto, B. I. Halperin, and Y.-S. Wu, Diophantine equation for the three-dimensional quantum Hall effect, Phys. Rev. B **45**, 13488 (1992).

[8] M. Koshino, H. Aoki, K. Kuroki, S. Kagoshima, and T. Osada, Hofstadter Butterfly and Integer Quantum Hall Effect in Three Dimensions, Phys. Rev. Lett. **86**, 1062 (2001).

[9] B. A. Bernevig, T. L. Hughes, S. Raghu, and D. P. Arovas, Theory of the Three-Dimensional Quantum Hall Effect in Graphite, Phys. Rev. Lett. **99**, 146804 (2007).

[10] H. L. Störmer, J. P. Eisenstein, A. C. Gossard, W. Wiegmann, and K. Baldwin, Quantization of the Hall Effect in an Anisotropic Three-Dimensional Electronic System, Phys. Rev. Lett. **56**, 85 (1986).

[11] J. R. Cooper, W. Kang, P. Auban, G. Montambaux, D. Jérome, and K. Bechgaard, Quantized Hall Effect and a New Field-Induced Phase Transition in the Organic Superconductor $(TMTSF)_2$ PF_6, Phys. Rev. Lett. **63**, 1984 (1989).

[12] S. T. Hannahs, J. S. Brooks, W. Kang, L. Y. Chiang, and P. M. Chaikin, Quantum Hall Effect in a Bulk Crystal, Phys. Rev. Lett. **63**, 1988 (1989).

[13] S. Hill, S. Uji, M. Takashita, C. Terakura, T. Terashima, H. Aoki, J. S. Brooks, Z. Fisk, and J. Sarrao, Bulk quantum Hall effect in $\eta - Mo_{4\ 11}$, Phys. Rev. B **58**, 10778 (1998).

[14] H. Masuda, H. Sakai, M. Tokunaga, Y. Yamasaki, A. Miyake, J. Shiogai *et al.*, Quantum Hall effect in a bulk antiferromagnet $EuMnBi_2$ with magnetically confined two-dimensional Dirac fermions, Sci. Adv. **2**, e1501117 (2016).

[15] F. Tang, Y. Ren, P. Wang, R. Zhong, J. Schneeloch, S. A. Yang, K. Yang, P. A. Lee, G. Gu, Z. Qiao *et al.*, Three-dimensional quantum Hall effect and metal-insulator transition in $ZrTe_5$, Nature (London) **569**, 537 (2019).

[16] F. Qin, S. Li, Z. Z. Du, C. M. Wang, W. Zhang, D. Yu, H.-Z. Lu, and X. C. Xie, Theory for the Charge-Density-Wave Mechanism of 3D Quantum Hall Effect, Phys. Rev. Lett. **125**, 206601 (2020).

[17] H. Li, H. Liu, H. Jiang, and X. C. Xie, 3D Quantum Hall Effect and a Global Picture of Edge States in Weyl Semimetals, Phys. Rev. Lett. **125**, 036602 (2020).

[18] S.-G. Cheng, H. Jiang, Q.-F. Sun, and X. C. Xie, Quantum Hall effect in wedge-shaped samples, Phys. Rev. B **102**, 075304 (2020).

[19] P. Wang, Y. Ren, F. Tang, P. Wang, T. Hou, H. Zeng, L. Zhang, and Z. Qiao, Approaching three-dimensional quantum hall effect in bulk $HfTe_5$, Phys. Rev. B **101**, 161201(R) (2020).

[20] Y. J. Jin, R. Wang, B. W. Xia, B. B. Zheng, and H. Xu, Three-dimensional quantum anomalous Hall effect in ferromagnetic insulators, Phys. Rev. B **98**, 081101(R) (2018).

[21] R. Chen, T. Liu, C. M. Wang, H.-Z. Lu, and X. C. Xie, Field-Tunable One-Sided Higher-Order Topological Hinge States in Dirac Semimetals, Phys. Rev. Lett. **127**, 066801 (2021).

[22] C. M. Wang, H.-P. Sun, H.-Z. Lu, and X. C. Xie, 3D Quantum Hall Effect of Fermi Arcs in Topological Semimetals, Phys. Rev. Lett. **119**, 136806 (2017).

[23] S. Li, C. M. Wang, Z. Z. Du, F. Qin, H.-Z. Lu, and X. C. Xie, 3D quantum Hall effects and nonlinear Hall effect, npj Quantum Mater. **6**, 96 (2021).

[24] H. M. Price, O. Zilberberg, T. Ozawa, I. Carusotto, and N. Goldman, Four-Dimensional Quantum Hall Effect with Ultracold Atoms, Phys. Rev. Lett. **115**, 195303 (2015).

[25] O. Zilberberg, S. Huang, J. Guglielmon, M. Wang, K. P. Chen, Y. E. Kraus, and M. C. Rechtsman, Photonic topological boundary pumping as a probe of 4D quantum Hall physics, Nature (London) **553**, 59 (2018).

[26] Z.-G. Chen, W. Zhu, Y. Tan, L. Wang, and G. Ma, Acoustic Realization of a Four-Dimensional Higher-Order Chern Insulator and Boundary-Modes Engineering, Phys. Rev. X **11**, 011016 (2021).

[27] Y. Wang, H. M. Price, B. Zhang, and Y. D. Chong, Circuit implementation of a four-dimensional topological insulator, Nat. Commun. **11**, 2356 (2020).

[28] R. Yu, Y. X. Zhao, and A. P. Schnyder, 4D spinless topological insulator in a periodic electric circuit, Natl. Sci. Rev. **7**, 1288 (2020).

[29] S.-C. Zhang, A Four-Dimensional Generalization of the Quantum Hall Effect, Science **294**, 823 (2001).

[30] M. Lohse, C. Schweizer, H. M. Price, O. Zilberberg, and I. Bloch, Exploring 4D quantum Hall physics with a 2D topological charge pump, Nature (London) **553**, 55 (2018).

[31] F. Terrier and F. K. Kunst, Dissipative analog of four-dimensional quantum Hall physics, Phys. Rev. Res. **2**, 023364 (2020).

[32] H. Weisbrich, R. L. Klees, G. Rastelli, and W. Belzig, Second Chern number and non-Abelian Berry phase in topological superconducting systems, PRX Quantum **2**, 010310 (2021).

[33] Y.-Q. Zhu, Z. Zheng, G. Palumbo, and Z. D. Wang, Topological Electromagnetic Effects and Higher Second Chern Numbers in Four-Dimensional Gapped Phases, Phys. Rev. Lett. **129**, 196602 (2022).

[34] X.-D. Chen, F.-L. Shi, J.-W. Liu, K. Shen, X.-T. He, C. T. Chan, W.-J. Chen, and J.-W. Dong, Second Chern crystals with inherently nontrivial topology, Natl. Sci. Rev. **10**, nwac289 (2022).

[35] X.-L. Qi, T. L. Hughes, and S.-C. Zhang, Topological field theory of time-reversal invariant insulators, Phys. Rev. B **78**, 195424 (2008).

[36] M. Mochol-Grzelak, A. Dauphin, A. Celi, and M. Lewenstein, Efficient algorithm to compute the second Chern number in four dimensional systems, Quantum Sci. Technol. **4**, 014009 (2018).

[37] S. Sugawa, F. Salces-Carcoba, A. R. Perry, Y. Yue, and I. B. Spielman, Second Chern number of a quantum-simulated non-Abelian Yang monopole, Science **360**, 1429 (2018).

[38] A. Zhang, Revealing Chern number from quantum metric, Chin. Phys. B **31**, 040201 (2022).

[39] Y. E. Kraus, Y. Lahini, Z. Ringel, M. Verbin, and O. Zilberberg, Topological States and Adiabatic Pumping in Quasicrystals, Phys. Rev. Lett. **109**, 106402 (2012).

[40] Y. E. Kraus, Z. Ringel, and O. Zilberberg, Four-Dimensional Quantum Hall Effect in a Two-Dimensional Quasicrystal, Phys. Rev. Lett. **111**, 226401 (2013).

[41] W. Zhang, F. Di, X. Zheng, H. Sun, and X. Zhang, Hyperbolic band topology with non-trivial second Chern numbers, Nat. Commun. **14**, 1083 (2023).

[42] A. Chen, Y. Guan, P. M. Lenggenhager, J. Maciejko, I. Boettcher, and T. Bzdušek, Symmetry and topology of hyperbolic Haldane models, Phys. Rev. B **108**, 085114 (2023).

[43] J. Li, R.-L. Chu, J. K. Jain, and S.-Q. Shen, Topological Anderson Insulator, Phys. Rev. Lett. **102**, 136806 (2009).

[44] H. Jiang, L. Wang, Q. F. Sun, and X. C. Xie, Numerical study of the topological Anderson insulator in HgTe/CdTe quantum wells, Phys. Rev. B **80**, 165316 (2009).

[45] C. W. Groth, M. Wimmer, A. R. Akhmerov, J. Tworzydło, and C. W. J. Beenakker, Theory of the Topological Anderson Insulator, Phys. Rev. Lett. **103**, 196805 (2009).

[46] B. Wu, J. Song, J. Zhou, and H. Jiang, Disorder effects in topological states: Brief review of the recent developments, Chin. Phys. B **25**, 117311 (2016).

[47] Y. Xing, L. Zhang, and J. Wang, Topological Anderson insulator phenomena, Phys. Rev. B **84**, 035110 (2011).

[48] C. P. Orth, T. Sekera, C. Bruder, and T. L. Schmidt, The topological Anderson insulator phase in the Kane-Mele model, Sci. Rep. **6**, 24007 (2016).

[49] H.-M. Guo, G. Rosenberg, G. Refael, and M. Franz, Topological Anderson Insulator in Three Dimensions, Phys. Rev. Lett. **105**, 216601 (2010).

[50] H. Guo, S. Feng, and S.-Q. Shen, Quantum spin Hall effect induced by nonmagnetic and magnetic staggered potentials, Phys. Rev. B **83**, 045114 (2011).

[51] R. Chen, D.-H. Xu, and B. Zhou, Topological Anderson insulator phase in a Dirac-semimetal thin film, Phys. Rev. B **95**, 245305 (2017).

[52] R. Chen, D.-H. Xu, and B. Zhou, Disorder-induced topological phase transitions on Lieb lattices, Phys. Rev. B **96**, 205304 (2017).

[53] R. Chen, C.-Z. Chen, J.-H. Sun, B. Zhou, and D.-H. Xu, Phase diagrams of Weyl semimetals with competing intraorbital and interorbital disorders, Phys. Rev. B **97**, 235109 (2018).

[54] R. Chen, D.-H. Xu, and B. Zhou, Floquet topological insulator phase in a Weyl semimetal thin film with disorder, Phys. Rev. B **98**, 235159 (2018).

[55] Y. Su, Y. Avishai, and X. R. Wang, Topological anderson insulators in systems without time-reversal symmetry, Phys. Rev. B **93**, 214206 (2016).

[56] L. Kimme and T. Hyart, Existence of zero-energy impurity states in different classes of topological insulators and superconductors and their relation to topological phase transitions, Phys. Rev. B **93**, 035134 (2016).

[57] C.-Z. Chen, J. Song, H. Jiang, Q.-F. Sun, Z. Wang, and X. C. Xie, Disorder and Metal-Insulator Transitions in Weyl Semimetals, Phys. Rev. Lett. **115**, 246603 (2015).

[58] C.-Z. Chen, H. Liu, H. Jiang, Q.-f. Sun, Z. Wang, and X. C. Xie, Tunable anderson metal-insulator transition in quantum spin-Hall insulators, Phys. Rev. B **91**, 214202 (2015).

[59] H. Shapourian and T. L. Hughes, Phase diagrams of disordered Weyl semimetals, Phys. Rev. B **93**, 075108 (2016).

[60] E. J. Meier, F. A. An, A. Dauphin, M. Maffei, P. Massignan, T. L. Hughes, and B. Gadway, Observation of the topological Anderson insulator in disordered atomic wires, Science **362**, 929 (2018).

[61] S. Stützer, Y. Plotnik, Y. Lumer, P. Titum, N. H. Lindner, M. Segev, M. C. Rechtsman, and A. Szameit, Photonic topological anderson insulators, Nature (London) **560**, 461 (2018).

[62] G.-G. Liu, Y. Yang, X. Ren, H. Xue, X. Lin, Y.-H. Hu, H.-x. Sun, B. Peng, P. Zhou, Y. Chong *et al.*, Topological Anderson Insulator in Disordered Photonic Crystals, Phys. Rev. Lett. **125**, 133603 (2020).

[63] X. Cui, R.-Y. Zhang, Z.-Q. Zhang, and C. T. Chan, Photonic $\mathbb{Z}_2$ Topological Anderson Insulators, Phys. Rev. Lett. **129**, 043902 (2022).

[64] X.-G. Li, H.-K. Xu, J.-H. Wang, L.-Z. Tang, D.-W. Zhang, C.-H. Yang, T. Su, C.-l. Wang, Z.-Y. Mi, W.-J. Sun *et al.*, Mapping a topology-disorder phase diagram with a quantum simulator, arXiv:2301.12138.

[65] Z.-Q. Zhang, B.-L. Wu, J. Song, and H. Jiang, Topological Anderson insulator in electric circuits, Phys. Rev. B **100**, 184202 (2019).

[66] D. N. Sheng, L. Sheng, and Z. Y. Weng, Quantum Hall effect in graphene: Disorder effect and phase diagram, Phys. Rev. B **73**, 233406 (2006).

[67] N. P. Mitchell, L. M. Nash, D. Hexner, A. M. Turner, and W. T. M. Irvine, Amorphous topological insulators constructed from random point sets, Nat. Phys. **14**, 380 (2018).

[68] T. Jiang, M. Xiao, W.-J. Chen, L. Yang, Y. Fang, W. Y. Tam, and C. T. Chan, Experimental demonstration of angular momentum-dependent topological transport using a transmission line network, Nat. Commun. **10**, 434 (2019).

[69] X. Cheng, J. Chen, L. Zhang, L. Xiao, and S. Jia, Antichiral edge states and hinge states based on the Haldane model, Phys. Rev. B **104**, L081401 (2021).

[70] R. Landauer, Electrical resistance of disordered one-dimensional lattices, Philos. Mag. **21**, 863 (1970).

[71] M. Büttiker, Absence of backscattering in the quantum Hall effect in multiprobe conductors, Phys. Rev. B **38**, 9375 (1988).

[72] D. S. Fisher and P. A. Lee, Relation between conductivity and transmission matrix, Phys. Rev. B **23**, 6851 (1981).

[73] T. A. Loring and M. B. Hastings, Disordered topological insulators via C*-algebras, Europhys. Lett. **92**, 67004 (2010).

[74] H. Huang and F. Liu, Theory of spin Bott index for quantum spin Hall states in nonperiodic systems, Phys. Rev. B **98**, 125130 (2018).

[75] E. Prodan, T. L. Hughes, and B. A. Bernevig, Entanglement Spectrum of a Disordered Topological Chern Insulator, Phys. Rev. Lett. **105**, 115501 (2010).

[76] E. Prodan, Disordered topological insulators: A non-commutative geometry perspective, J. Phys. A: Math. Theor. **44**, 113001 (2011).

[77] R. Bianco and R. Resta, Mapping topological order in coordinate space, Phys. Rev. B **84**, 241106(R) (2011).

[78] O. Pozo, C. Repellin, and A. G. Grushin, Quantization in Chiral Higher Order Topological Insulators: Circular Dichroism and Local Chern Marker, Phys. Rev. Lett. **123**, 247401 (2019).

[79] Y.-F. Zhang, Y.-Y. Yang, Y. Ju, L. Sheng, R. Shen, D.-N. Sheng, and D.-Y. Xing, Coupling-matrix approach to the Chern number calculation in disordered systems, Chin. Phys. B **22**, 117312 (2013).

[80] A. Kitaev, Anyons in an exactly solved model and beyond, Ann. Phys. **321**, 2 (2006).

[81] J. H. García, L. Covaci, and T. G. Rappoport, Real-Space Calculation of the Conductivity Tensor for Disordered Topological Matter, Phys. Rev. Lett. **114**, 116602 (2015).

[82] A. Weiße, G. Wellein, A. Alvermann, and H. Fehske, The kernel polynomial method, Rev. Mod. Phys. **78**, 275 (2006).

[83] D. Varjas, M. Fruchart, A. R. Akhmerov, and P. M. Perez-Piskunow, Computation of topological phase diagram of disordered $Pb_{1-x}Sn_xTe$ using the kernel polynomial method, Phys. Rev. Res. **2**, 013229 (2020).

[84] H.-M. Guo, Topological invariant in three-dimensional band insulators with disorder, Phys. Rev. B **82**, 115122 (2010).

[85] M. J. Puska, S. Pöykkö, M. Pesola, and R. M. Nieminen, Convergence of supercell calculations for point defects in semiconductors: Vacancy in silicon, Phys. Rev. B **58**, 1318 (1998).

[86] T. B. Boykin, N. Kharche, G. Klimeck, and M. Korkusinski, Approximate bandstructures of semiconductor alloys from tight-binding supercell calculations, J. Phys.: Condens. Matter **19**, 036203 (2007).

[87] C. Freysoldt, J. Neugebauer, and C. G. Van de Walle, Fully *Ab Initio* Finite-Size Corrections for Charged-Defect Supercell Calculations, Phys. Rev. Lett. **102**, 016402 (2009).

[88] P. A. Schultz, Theory of Defect Levels and the "Band Gap Problem" in Silicon, Phys. Rev. Lett. **96**, 246401 (2006).

[89] J. Dong, V. Juričić, and B. Roy, Topolectric circuits: Theory and construction, Phys. Rev. Res. **3**, 023056 (2021).

[90] X. Chen, A. Tiwari, and S. Ryu, Bulk-boundary correspondence in (3+1)-dimensional topological phases, Phys. Rev. B **94**, 045113 (2016).

[91] R. S. K. Mong and V. Shivamoggi, Edge states and the bulk-boundary correspondence in Dirac Hamiltonians, Phys. Rev. B **83**, 125109 (2011).

[92] M. B. Hastings and T. A. Loring, Almost commuting matrices, localized Wannier functions, and the quantum Hall effect, J. Math. Phys. **51**, 015214 (2010).